JGR Planets

RESEARCH ARTICLE
10.1029/2022JE007593

Cryogenic Sulfuric Weathering and Challenges for Preserving Iron-Rich Olivine on Cold and Icy Mars

Xiao-Wen Yu[1,2], Yu-Yan Sara Zhao[3,4], Yanxue Wu[5], Chao Qi[6], Dongdong Li[7], Honglei Lin[6], Shiling Yang[8], Jianzhong Liu[1,4], and Xiongyao Li[1,4]

[1]Center for Lunar and Planetary Sciences, Institute of Geochemistry Chinese Academy of Sciences, Guiyang, China, [2]College of Earth and Planetary Sciences, University of Chinese Academy of Sciences, Beijing, China, [3]International Center for Planetary Science, College of Earth Science, Chengdu University of Technology, Chengdu, China, [4]CAS Center for Excellence in Comparative Planetology, Hefei, China, [5]Analysis and Test Center, Guangdong University of Technology, Guangzhou, China, [6]Key Laboratory of Earth and Planetary Physics, Institute of Geology and Geophysics, Chinese Academy of Sciences, Beijing, China, [7]Key Laboratory of Comprehensive and Highly Efficient Utilization of Salt Lake Resources, Qinghai Institute of Salt Lakes, Chinese Academy of Sciences, Xining, China, [8]Key Laboratory of Cenozoic Geology and Environment, Institute of Geology and Geophysics, Chinese Academy of Sciences, Beijing, China

Key Points:

- Forsterite-dominant olivine dissolves stoichiometrically, but the dissolution of fayalite in Fa-dominant olivine is hindered
- Fe-rich olivine alteration primarily produces Fe^{II}-Mg-sulfates and amorphous silica, with minor ferric sulfates and gypsum
- Fe-rich olivine lasts 10s to 100s of years and restricting acid-olivine interactions is essential for preserving olivine on cold and icy Mars

Supporting Information:

Supporting Information may be found in the online version of this article.

Correspondence to:

Y.-Y. S. Zhao,
zhaoyuyan@cdut.edu.cn

Citation:

Yu, X.-W., Zhao, Y.-Y. S., Wu, Y., Qi, C., Li, D., Lin, H., et al. (2023). Cryogenic sulfuric weathering and challenges for preserving iron-rich olivine on cold and icy Mars. *Journal of Geophysical Research: Planets*, *128*, e2022JE007593. https://doi.org/10.1029/2022JE007593

Received 28 SEP 2022
Accepted 17 DEC 2022

Author Contributions:

Conceptualization: Yu-Yan Sara Zhao, Shiling Yang, Jianzhong Liu, Xiongyao Li
Funding acquisition: Shiling Yang, Jianzhong Liu, Xiongyao Li
Investigation: Xiao-Wen Yu, Yanxue Wu, Dongdong Li, Honglei Lin
Resources: Chao Qi
Supervision: Yu-Yan Sara Zhao, Shiling Yang, Jianzhong Liu, Xiongyao Li
Visualization: Xiao-Wen Yu
Writing – original draft: Xiao-Wen Yu, Yu-Yan Sara Zhao
Writing – review & editing: Xiao-Wen Yu, Yu-Yan Sara Zhao, Yanxue Wu, Chao Qi, Dongdong Li, Honglei Lin, Shiling Yang, Jianzhong Liu, Xiongyao Li

Abstract Iron-rich olivine (Fe contents ≥20%) is widely distributed on Mars, but its dissolution rates, weathering products, and particularly Fe behavior under Mars-relevant conditions are largely unconstrained. Here, we experimentally investigate the dissolution of synthetic Fe-rich olivine (Fa_{29} to Fa_{100}; grain size ~53 μm) for a water-limited cryogenic sulfuric weathering scenario at 233 K. Fayalite (Fa) and forsterite (Fo) in Fo-dominant olivine dissolve simultaneously, whereas fayalite dissolution in Fa-dominant olivine is hindered. Primary alteration products are Fe^{II}-Mg-sulfates and amorphous silica with minor ferric sulfates and gypsum. Freezing and acidic conditions enhance Fe mobility and subsequent Fe cycling on Mars. The lifetime of Fe-rich olivine is two to three orders of magnitude shorter than that of Mg-rich San Carlos olivine. The cryogenic sulfuric weathering scenario greatly challenges the survival of Fe-rich olivine. Spatial and temporal restrictions for acid-olivine interactions or insufficient sulfur supply relative to olivine are essential to preserving olivine throughout cold and icy ancient Mars.

Plain Language Summary Cryogenic sulfuric weathering is proposed for forming large-scale layered sulfate deposits on Mars, such as Meridiani Planum and Valles Marineris. In particular, olivine dissolution is essential for producing these evaporative sulfate assemblages. Although qualitatively likely, how Fe-rich olivine, widely distributed in Martian basaltic crusts, would respond to the cryogenic sulfuric weathering scenario is currently unknown. We synthesized Fe-rich olivine samples (Fa_{29} ~ Fa_{100}) and investigated their dissolution processes and alteration products under sulfuric acidic conditions at 233 K. We found that forsterite and fayalite in Fo-dominant olivine (Fa# ≤ 50) dissolve simultaneously, whereas the dissolution of fayalite in Fa-dominant olivine (Fa# > 50) is hindered. Primary alteration products are Fe^{II}-Mg-sulfates and amorphous silica with minor ferric sulfates and gypsum. Freezing and acidic conditions enhance Fe mobility and subsequent Fe cycling on Mars. Fe-rich olivine dissolves two to three orders of magnitude faster than Mg-rich San Carlos olivine, and 0.1 mm Fe-rich olivine grains can survive only 10s to 100s of years under H_2SO_4-233 K conditions. The cryogenic sulfuric weathering scenario greatly challenges the survival of Fe-rich olivine. Thus, spatial and temporal restrictions for acid-olivine interactions or insufficient sulfur supply relative to olivine are essential for preserving olivine throughout cold and icy ancient Mars.

1. Introduction

Olivine ($(Mg, Fe)_2SiO_4$) is widely distributed on the Martian surface (Koeppen & Hamilton, 2008). Unlike Earth, olivine on Mars is generally iron-rich (i.e., Fa# > 20; Fa# is mol% of fayalite in the forsterite (Fo)-fayalite (Fa) solid solution). From the orbit, a wide range of Fa# values are suggested for Martian olivine ($Fa_{9\text{-}61}$; most commonly $Fa_{32\text{-}47}$), and those formed early are Mg-rich, whereas those formed later are more Fe-rich (Koeppen & Hamilton, 2008). At the landing sites, normative olivine composition of Gusev rocks is $Fa_{27\text{-}58}$ (McSween et al., 2008). At Meridiani Planum, olivine is absent in the sedimentary outcrop of the Burns Formation, but the basaltic sands, likely to represent regional composition, contain olivine as Fa_{40} (Christensen et al., 2004). In Nili Fossae, where the Jezero Crater is located close by, olivine has a range of $Fa_{30\text{-}70}$ (Hoefen et al., 2003). Olivine

in the Martian meteorites is in the range of Fa_{21-34} in shergottites, Fa_{58-85} in nakhlites, and Fa_{20-32} in chassignites (McSween, 2015).

Olivine is likely the primary rock-forming mineral to dissolve during acidic aqueous weathering of the Martian basaltic crust (Burns, 1993; Hurowitz et al., 2006). Many studies have examined forsterite (San Carlos olivine, Fa_{09}) alteration under Mars-relevant conditions (Dehouck et al., 2014; Gaudin et al., 2018; Hausrath & Brantley, 2010) with a few including synthetic fayalite (Hausrath & Brantley, 2010), and concluded that fayalite preferentially dissolves approximately 10 times faster than forsterite under the same deoxygenated conditions (Hausrath & Brantley, 2010; Stopar et al., 2006). However, due to the lack of natural Fe-rich olivine on Earth, dissolution rates, characteristics of alteration products, and particularly the Fe behavior during weathering Fo-Fa solid solution series are largely unconstrained.

In recent years, more evidence has suggested cold and icy early Mars during the late Noachian toward the Hesperian, with only sporadic, short-term warm and wet environments (Bishop et al., 2018; Fastook & Head, 2015; Wordsworth, 2016). Under the cold and icy conditions, volcanic aerosols (carriers of oxidized sulfur species) and pyroclastic volcanic dust may contribute to massive ice deposits and potentially enable sulfuric weathering under cryogenic conditions. Although the low temperature is generally considered to slow dissolution kinetics and result in a prolonged lifetime of the olivine particles (Olsen & Rimstidt, 2007; Stopar et al., 2006), freezing acidic sulfuric solutions sufficiently concentrates the sulfuric acids by removing water as ice and may efficiently promote the dissolution rates under low T conditions. Cryogenic sulfuric weathering mechanism has been proposed to account for the formation of large-scale layered sulfate deposits on Mars, such as Meridiani Planum and Valles Marineris (Michalski & Niles, 2012; Niles & Michalski, 2009; Niles et al., 2017). A recent discovery of spontaneous jarosite particles (micron or submicron in size) in the Earth's Antarctic ice core is considered to support the proposed sulfuric cryogenic weathering scenario on Mars (Baccolo et al., 2021). In addition, ferric sulfate brines are proposed to be candidates for low-temperature aqueous activity on Mars, given their eutectic temperature as low as 205 K and slow evaporation rates (Chevrier & Altheide, 2008). The ubiquitous formation and activity of ferric sulfate brines make them a likely weathering agent over the modern Martian surface; however, the weathering effects and alteration products of acidic ferric sulfate brines on rock-forming minerals are less explored.

In this study, we experimentally examine the dissolution of synthetic Fe-rich olivine (Fa_{100}, Fa_{71}, Fa_{50}, and Fa_{29}; grain size ~53 μm) under a water-limited cryogenic sulfuric weathering scenario. Both H_2SO_4 and acidic Fe^{III}-SO_4 solutions were examined at 233 K for 100 days. The new results provide essential constraints on Fe-rich olivine weathering on "cold and icy" ancient Mars. Note that in addition to the cryogenic sulfuric weathering scenario, other fluid-rock interactions, such as aqueous alteration under the Martian CO_2 atmosphere or hydrothermal alterations in the subsurface, are also important in producing diverse secondary minerals observed in the Martian crusts, which are beyond the scope of this paper and will be presented in subsequent series of works.

2. Materials and Methods

2.1. Synthesis of Initial Fe-Rich Olivine Samples

The fayalite (Fa_{100}) sample was synthesized in the furnace using powders of Fe_2O_3 and SiO_2 in a molar ratio of 1:1.002 at temperatures close to the melting point of fayalite under a controlled oxygen buffer (using a gas mixture of CO_2 and CO). The samples of ~Fa_{30}, ~Fa_{50}, and ~Fa_{70} were then fabricated from mixtures of the synthesized fayalite and natural San Carlos olivine. The mixtures were ground to a particle size of <10 μm and annealed at 1670 K in a furnace for 16 hr under a controlled oxygen buffer (Qi et al., 2021; Zhao et al., 2009). The synthesized olivine was further ground and sieved to ~53 μm as the initial samples in the batch experiments.

The initial synthetic Fe-rich olivine samples were characterized using powder X-ray diffraction (XRD) and scanning electron microscopy (SEM) with energy dispersive X-ray spectrometry (EDS). Powder XRD data were collected using a Panalytical Empyrean diffractometer at 45 kV and 40 mA with Cu–Ka radiation ($\lambda = 1.5419$ Å). Data were collected between 10°~ and 60° 2θ, with a scan step of 0.0263° and 36.465 s of counting time per step. The SEM/EDS measurements were taken using an FEI Scios at 5 kV. The specific surface area of synthetic Fe-rich olivine samples was measured using a five-point Brunauer–Emmett–Teller nitrogen isotherm method. The initial chemical composition of Fe-rich olivine was determined by an inductively coupled plasma emission spectrometer (ICP735-ES) after acid digestion.

2.2. Batch Experiments in H_2SO_4 at 233 K

To ensure comparison, the settings of the H_2SO_4-233 K experiments were similar to those of Niles et al. (2017). Ten grams of acid-washed glass beads (~400 μm in size) were added to a 50 mL antifreeze Teflon tube. Then, the tube was moved to a glove box filled with CO_2 gas (1 bar), and 0.5 mL of 0.5 M H_2SO_4 solution was added. The H_2SO_4 solution (pH 0.96 at room temperature) was prepared with deoxygenated ultrapure water (18 MΩ, dissolved $O_2 \leq 1$ ppm). Then, the tubes were put into the freezer at 233 K for 2 hr. After that, 50 mg of olivine powder (grain size ≤53 μm) was added to each frozen tube. The tubes were shaken vigorously with a vortex mixer for 1 min to mix all the reactants and immediately transferred back to the freezer for the batch experiments.

A total of eight parallel tubes were prepared for each type of olivine (Fa_{29}, Fa_{50}, Fa_{71}, and Fa_{100}; ~53 μm), and one tube was removed every 20 days for a total of 100 days for solution sample analysis. On the 20th, 60th, and 100th days, one tube was removed for solid sample analysis. For the solution sample analysis, 10 mL of 0.1 M sodium acetate solution was added to the tube, and the tube was capped and shaken vigorously for 30 s with a vortex mixer. Then, the supernatant was sampled and filtered with a 0.22 μm Nalgene filter membrane and measured immediately for solution compositions. For the solid sample analysis, the reactants in tubes were directly freeze-dried (at 233 K; 12 hr) without adding additional reagents.

2.3. Batch Experiments in Ferric Sulfate Solution at 233 K

The ferric sulfate solution (0.97 M, pH 0.41 at room temperature) was prepared by dissolving 31 g of ferric sulfate ($Fe_2(SO_4)_3 \cdot xH_2O$, 97%, Sigma) in 80 g of ultrapure water. Then, 200 mg (grain size ≤53 μm) of Fe-rich olivine samples (i.e., Fa_{50} and Fa_{71}) and 2 mL ferric sulfate solution were added to the antifreeze Teflon tube, making a W/R ratio of 10. The mixtures were vigorously mixed with a vortex mixer for 30 s and immediately transferred to the freezer set at 233 K.

A total of five parallel tubes were prepared for each type of olivine. Each tube was removed every 20 days for a total of 100 days during batch experiments. The frozen tube was removed from the freezer and thawed at room temperature for 30 min, and the supernatant samples were sampled and filtered with a 0.22 μm Nalgene filter. The remaining solid sample was washed twice with deoxygenated ultrapure water and then freeze-dried.

During the entire experiment, we did not deliberately isolate samples to anoxic atmospheric conditions except for using deoxygenated ultrapure water (18 MΩ, dissolved $O_2 \leq 1$ ppm) for making solutions and washing samples. The deoxygenated ultrapure water was prepared by boiling ultrapure water and simultaneously introducing nitrogen gas into the water. The frozen conditions provided a deoxygenated environment for the reactants in the tubes (Niles et al., 2017).

2.4. Sample Analysis

The solution samples were analyzed immediately after sample collection. Atomic absorption spectrophotometry (AAS) was used to measure Fe_T and Mg^{2+} concentrations during olivine dissolution. The samples were diluted 20 times to reduce salinity before analysis. The AAS measurements were first calibrated using brine-free standards (2 mg/kg Fe_T and 1 mg/kg Mg^{2+}) and then using a set of matrix-matched standards prepared using brines to mimic the actual samples. All the standards were acidified with 4 wt% nitric acid. The detection limit of Fe_T and Mg^{2+} in the matrix-matched standard was 0.1 mg/kg. The standard error averaged ±1.32%. During sample measurements, the standards were measured at intervals of every eight samples. A plasma emission spectrometer (Vista Pro ICP-OES) was used to determine the concentration of Si^{4+}, K^+, and Ca^{2+} ions released during olivine dissolution. The OES was calibrated using standards (2 mg/kg Si, 2 mg/kg K, and 2 mg/kg Ca), and the standard error averaged ±1.74%. During sample measurements, the standards were measured at intervals of every 10 samples.

The final solid products were acquired by XRD patterns of an X-ray diffractometer (Panalytical X'pert PRO MPD) using an X-ray source of Cu-Kα ($\lambda = 0.154$ nm) in two-theta/omega scanning mode with a scan range of 10°–60° and a scan rate of 0.01° s^{-1}. In addition, the final reaction products were carefully characterized by SEM with EDS and a high-resolution field emission transmission electron microscope (FEI Talos F200S).

Table 1
Characteristics of Synthetic Initial Fe-Rich Olivine Samples

Fa#	Specific surface area (cm^2/g)	Compositions (wt%)						
		FeO	MgO	SiO_2	Al_2O_3	CaO	MnO	Ni
Fa29	1,295	26.3	35.8	35.9	0.26	0.32	0.11	0.23
Fa50	1,475	41.6	23.3	33.2	0.19	0.24	0.16	0.08
Fa71	1,249	54.8	12.5	31.0	0.07	0.22	0.05	0.06
Fa100	3,592	70.9	0.01	27.8	0.06	0.25	0.03	0.03

Note. Fa# = $Fe_{mol}/(Fe_{mol} + Mg_{mol}) \times 100$.

2.5. Dissolution Rate Calculation

The released cation concentrations in solution versus time (s) derivative produced the initial dissolution rate at $t = 0$ (Rimstidt & Newcomb, 1993). The rates were then normalized using the specific surface area and mass of olivine in each experiment to yield the standard initial dissolution rate r (mol cm^{-2} s^{-1}), which enables comparison across different olivine samples in this study and with previous studies. We examined Mg, Fe, and Mg + Fe for Fa_{29}, Fa_{50}, and Fa_{71} in H_2SO_4-233 K.

In addition, a shrinking sphere model (Lasaga, 1998) was used to estimate the lifetime of a 0.1-mm olivine particle.

$$\Delta t = \frac{d}{2V_m r}$$

where Δt is the lifetime of the particle (s), d is the diameter of the particle (cm), V_m is the molar volume of the mineral (cm^3 mol^{-1}), and r is the initial dissolution rate (mol cm^{-2} s^{-1}). The shrinking sphere model assumes that the particles interact with the ambient solution and dissolve without interruption. The 0.1-mm particle size was chosen for comparison with previous studies (Niles et al., 2017).

3. Results and Discussion

3.1. Characteristics of Initial Fe-Rich Olivine

Synthetic Fe-rich olivine samples (Fa_{100}, Fa_{71}, Fa_{50}, and Fa_{29}) are pure and well-crystalline as confirmed by X-ray powder differentiation (XRD) (Figure S1 in Supporting Information S1). Characteristic peaks of the XRD show a gradual transition from the Fo-dominant olivine (Fa_{29}) to the fayalite endmember (Fa_{100}). Acidic digestion analysis shows that the synthetic olivine samples primarily contain FeO, MgO, and SiO_2 with minor Al_2O_3, CaO, MnO, and Ni contents (Table 1). The olivine samples were ground and sieved for grain sizes <53 μm for the batch experiments. The specific surface areas of the olivine samples were obtained (Table 1) and used for calculating the initial dissolution rates. The average composition of acid-washed silica beads (grain size ~400 μm) used in H_2SO_4-233 K experiments are SiO_2 (63.5% ± 11.1%), Na_2O (17.1% ± 1.7%), MgO (8.4% ± 2.3%), and CaO (6.4% ± 2.9%) with minor Al_2O_3 (1.2% ± 1.4%) (Table S1 in Supporting Information S1).

3.2. Stoichiometric Dissolution of Fo-Dominant Olivine and Incongruent Dissolution of Fa-Dominant Olivine

In the H_2SO_4-233 K experiments, Fe_T and Mg were released and accumulated in the solutions as the Fe-rich olivine (Fa_{100}, Fa_{71}, Fa_{50}, and Fa_{29}) dissolved (Figures 1a and 1b). At the end of the Fa_{29} and Fa_{50} experiments, Fe_T decreased slightly from the solution (Figure 1a), suggesting a slight removal of Fe from the solution. The Si in the solution was approximately two orders of magnitude lower than Fe_T and Mg and varied for a similar range across different types of olivine (Figure 1c).

The dissolution of Fo-Fa solid solution is generally congruent under water-limited cryogenic conditions. For Fo-dominant olivine (Fa# ≤ 50; Fa_{29} and Fa_{50}), the Fe_T/Mg molar ratios released in the solution were stoichiometric (Figure 1d). For Fa-dominant olivine (Fa# > 50; Fa_{71}), Fe_T/Mg molar ratios in the solution were constantly lower than those of the initial olivine (Figure 1d). Because the released Fe_T concentrations in the solution of the Fa_{71} experiments were at the same level as those of the Fa_{50} experiments (Figure 1a), the lower Fe_T/Mg ratios are primarily due to hindered dissolution of the fayalite endmember. Some unknown factors at the olivine-solution interfaces might hinder fayalite dissolution in Fa-dominant olivine. Nevertheless, the initial Fa# of olivine has a fundamental influence on Fe leaching, which would ultimately be reflected in the Fe/Mg ratios of the leachate and secondary mineral assemblages.

In the Fe^{III}-SO_4-233 K experiments, Fa_{50} and Fa_{71} were examined for comparison with the H_2SO_4-233 K experiments. Since abundant Fe^{III} was initially present, we only monitored the released Mg and Si throughout the experiments. The trends of Mg and Si release were similar to those of the H_2SO_4 experiments, but the concentrations were about one order of magnitude lower (Figures 1e and 1f), suggesting a lower fraction of altered olivine in

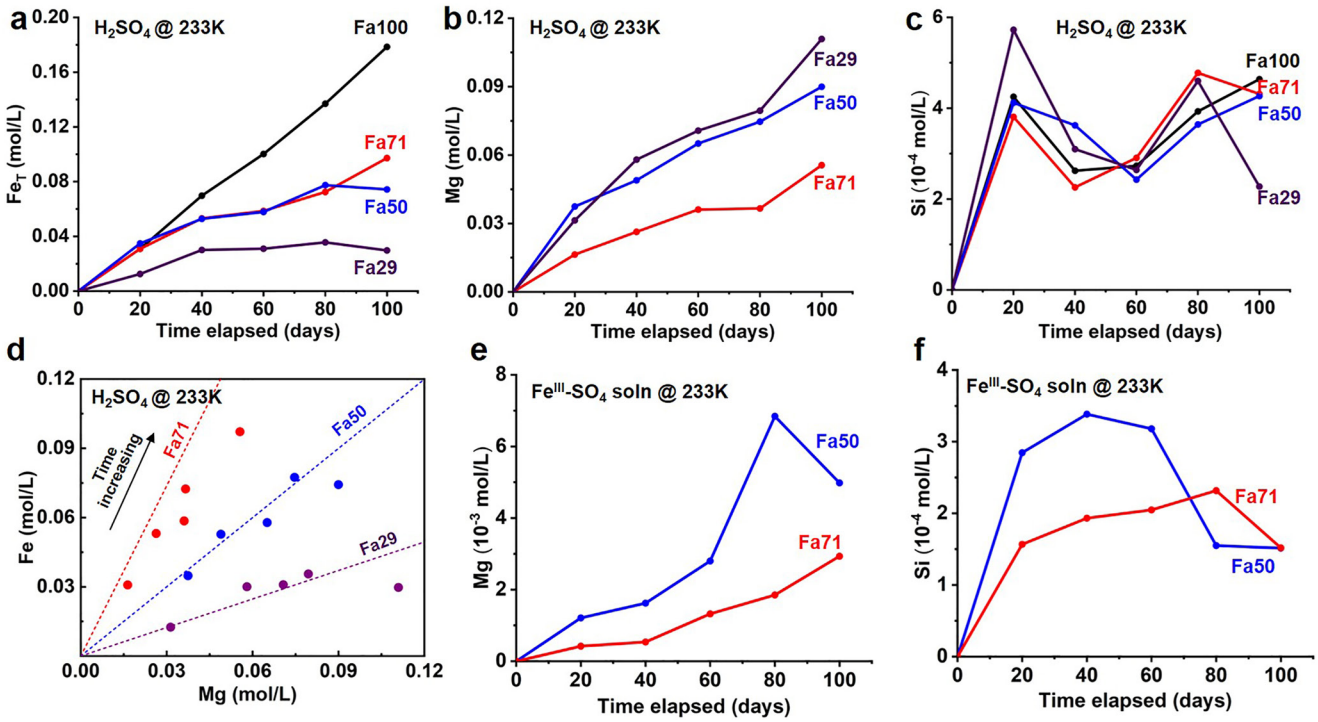

Figure 1. Released Fe_T, Mg, and Si into the solutions during olivine dissolution in H_2SO_4-233 K and Fe^{III}-SO_4-233 K experiments. Colors represent olivine type as Fa_{100} (in black), Fa_{71} (in red), Fa_{50} (in blue), and Fa_{29} (in purple). In H_2SO_4-233 K experiments, (a) Fe_T and (b) Mg generally showed congruent release for all four olivine samples. At the end of the Fa_{29} and Fa_{50} experiments, Fe_T showed a slight decrease, suggesting a phase change of Fe in the solution. (c) Si in the solution was approximately two orders of magnitude lower than Fe_T and Mg, and varied within a similar range across different types of olivine. (d) Comparison of Fe_T and Mg released into the solutions versus those of initial olivine samples in Fa_{29}, Fa_{50}, and Fa_{71} experiments under H_2SO_4-233 K. Dashed lines and dots in the same color represent Fe_T/Mg molar ratios of the initial olivine and released in the solution, respectively. For Fa_{29} and Fa_{50} (Fo-dominant olivine), the dissolution of olivine was congruent and the Fe_T/Mg molar ratios in the solution were consistent with those of the initial olivine. For Fa_{71} (Fa-dominant olivine), the Fe_T/Mg molar ratios in the solution were lower than those of the initial olivine, indicating that fayalite dissolution was hindered. Fa_{100} contained negligible Mg and thus was not considered. (e) Mg and (f) Si concentrations in the solution during Fa_{50} and Fa_{71} dissolution in the Fe^{III}-SO_4-233 K experiments. Since Fe was initially present in the solution, only Mg and Si were monitored throughout the experiments. The general trends of Mg and Si release were similar to those of the H_2SO_4 experiments.

these experiments. Estimations using released Mg^{2+} in the solution suggest that only 0.9% of Fa_{50} and Fa_{71} were altered in the Fe^{III}-SO_4-233 K experiments, substantially lower than those of H_2SO_4-233 K experiments (e.g., 15.4% of Fa_{50} and 17.8% of Fa_{71}).

3.3. Formation of Fe^{II}-Mg-Sulfates, Fe^{III}-Sulfates, Gypsum, and Amorphous Silica

In H_2SO_4-233 K experiments, two primary secondary phases after freeze-drying were evaporative sulfates and amorphous silica. Fa_{100} olivine produced ferrous- and ferric-sulfates with Fe/S molar ratios of 1:1 and 2:3, respectively (Figure 2a). The formed ferrous sulfates had a pseudo-crystalline shape but were amorphous inside (Figure 2b). The Fo-Fa solid solution olivine (i.e., Fa_{71}, Fa_{50}, and Fa_{29}) mainly produced Fe^{II}-Mg sulfates, confirmed by (Fe_T + Mg)/S molar ratios of 1:1 (Figures 2d–2h). Due to the coexisting Mg in these sulfates, we cannot determine whether any Fe^{III} was present, but Fe^{II} should be the primary species in freezing and deoxygenated aqueous conditions (Niles et al., 2017). Also, the Fe_T/Mg molar ratios in the produced sulfates were consistent with the solution concentrations, suggesting that Fe primarily presents as Fe^{II} and substitutes with Mg^{2+}. Amorphous Fe^{II}-Mg sulfates are likely formed due to fast sublimation and low-*T* conditions. High hydration states were expected for these precipitated sulfates under freezing conditions (Marion et al., 2008), but we cannot constrain the hydration states by electron microscopy. Amorphous silica was ubiquitous and mixed with sulfates and olivine grains in all experiments (Figures 2f and 2h). Minor well-crystalline gypsum ($CaSO_4{\cdot}2H_2O$) was observed in the final evaporites of the Fa_{100} and Fa_{71} experiments (Figures 2a and 2c). The source of Ca^{2+} may originate from olivine as a minor component (Table 1).

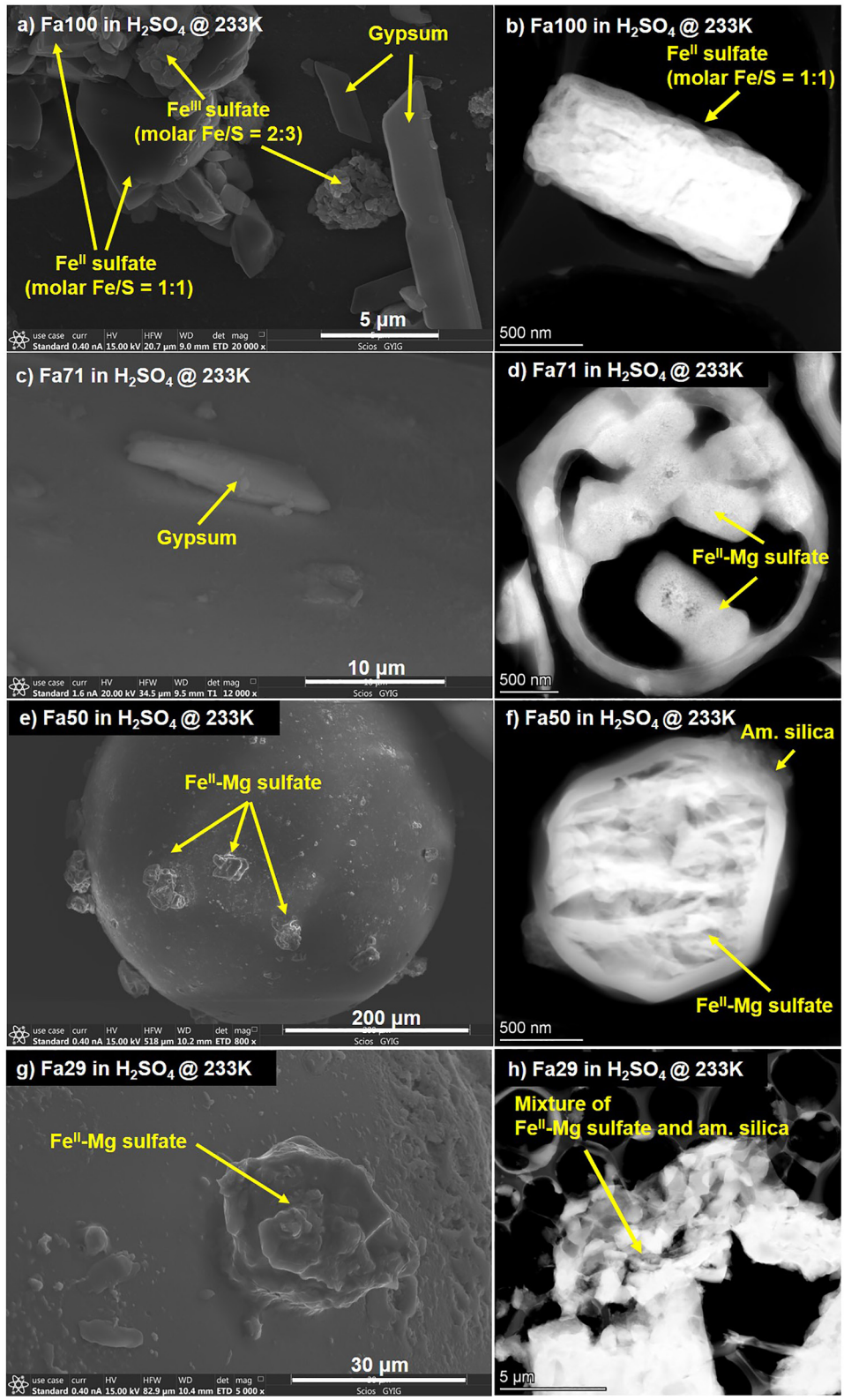

Figure 2.

Table 2
The Standard Initial Dissolution Rates and Calculated Particle Lifetimes of Olivine Samples With Different Fa# Values (Grain Size 0.1 mm)

	In H_2SO_4 @ 233 K (pH 0.96 @ 298 K)						In Fe^{III}-SO_4 soln @ 233 K (pH 0.41 @ 298 K)		
Fa#	Log *r*-Mg (mol cm^{-2} s^{-1})	Log *r*-Fe_T (mol cm^{-2} s^{-1})	Log *r*-Mg + Fe_T (mol cm^{-2} s^{-1})	Δ*t*-Mg (yr)	Δ*t*-Fe (yr)	Δ*t*-(Mg + Fe) (yr)	Log *r*-Mg (mol cm^{-2} s^{-1})[d]	Δ*t* (yr)	Notes
Fa100	n.a.	−9.93	−9.93[a]	n.a.	0.03	0.03[a]	–	–	This study
Fa71	−10.09	−9.85	−9.65	0.04	0.02	0.02	−11.23	0.59	This study
Fa50	−9.99	−10.09	−9.74	0.03	0.04	0.02	−11.11	0.45	This study
Fa29	−9.79	−10.45[b]	−9.71	0.02	0.10	0.02	–	–	This study
Fa09[c]			−12.17			5.29			Niles et al. (2017)

Note. Log *r*-Mg, log *r*-Fe_T, and log *r*-Mg + Fe_T are dissolution rates obtained using released Mg, Fe_T or the sum of Mg + Fe_T in the solution, respectively. "n.a." represents not available.

[a]Log *r* and Δ*t* of the sum of (Mg + Fe_T) for Fa_{100} were considered the same as those using Fe_T because the concentrations of released Mg are in the mg/kg level, making Mg + Fe_T ≈ Fe_T. [b]Log *r*-Fe_T of Fa_{29} was based on a low R^2 (0.51) compared to other data sets ($R^2 \geq 0.90$) (Figure S4d in Supporting Information S1); in comparison, log *r*-Mg has better confidence. [c]Fa_{09} data (Niles et al., 2017) are calculated using the sum of Mg + Fe_T. Caution must be taken in choosing the cations for calculating the rates of Fo-Fa samples since Mg, Fe_T and Mg + Fe_T may result in slightly different results. [d]Note that only Mg can be used to estimate the dissolution rates for the Fe^{III}-SO_4-233 K experiments due to the abundant Fe initially present in the ferric sulfate solution.

In the Fe^{III}-SO_4-233 K experiments, the dissolution of Fa_{50} and Fa_{71} was expected to produce similar secondary phases as in the H_2SO_4-233 K experiments. Because the final products were thoroughly washed with deoxygenated water to remove soluble sulfates initially present in the Fe^{III}-SO_4-233 K experiments, amorphous silica was the primary observable secondary product covering olivine grains (Figure S3 in Supporting Information S1). Gypsum was not observed in the final products.

3.4. Fast Dissolution Rates and Short Lifetimes of Fe-Rich Olivine

Figure S4 in Supporting Information S1 shows linear fitting for equations to calculate the initial dissolution rates in all the experiments. Previously reported olivine dissolution rates were based on either released Mg or Mg + Fe concentrations (Hausrath & Brantley, 2010; Niles et al., 2017). However, we find that for Fo-Fa solid solutions under H_2SO_4-233 K conditions, using Mg, Fe_T, or Mg + Fe_T may result in slightly different dissolution rates and trends. The initial dissolution rates (log r) of Fa_{71}, Fa_{50}, and Fa_{29} obtained from Mg ranged from −10.09 to −9.79, those obtained from Fe_T ranged from −9.85 to −10.20, and those obtained from Mg + Fe_T ranged from −9.65 to −9.93 (Table 2). Increasing Fa# from Fa_{29} to Fa_{71}, the dissolution rates estimated using Mg show a decreasing trend, while those estimated using Fe_T show an increasing trend. The rates calculated using Mg + Fe_T are faster than those using Mg or Fe_T and represent the maximum dissolution rates. Fe-rich olivine dissolves two to three orders of magnitude faster than Mg-rich olivine (San Carlos olivine; Fa_{09}) under comparable experimental conditions (Table 2). However, interestingly, Fa_{71} dissolves faster than Fa_{100} (using both Fe_T and Mg + Fe_T for calculation) and counters from the long-term presumption that fayalite and forsterite endmembers bracket the dissolution rates of Fo-Fa solid solution series. Our newly obtained dissolution rates under H_2SO_4-233 K are at the same level as the maximum dissolution rates estimated by numerical simulations for aqueous conditions of pH 2 and 373 K and substantially faster than those extrapolated for pH 2 and 223 K conditions (Stopar et al., 2006).

Under Fe^{III}-SO_4-233 K conditions, the dissolution rates of Fa_{50} and Fa_{71} (estimated using Mg only) show relatively slower dissolution rates ranging from −11.23 to −11.11 than those under H_2SO_4-233 K conditions (Table 2). Although the acidic ferric sulfate solution has an initially lower pH (0.41 at 298 K) than the H_2SO_4 solution (pH

Figure 2. Scanning electron microscopy (SEM)-energy dispersive X-ray spectrometry (EDS) and transmission electron microscope (TEM)-EDS analysis of the secondary phases in the H_2SO_4-233 K experiments after freeze-drying. (a) Fe-sulfates and gypsum were identified in the Fa_{100} experiment. Both ferrous and ferric sulfates can be observed with molar Fe/S ratios of 1:1 (ferrous) and 2:3 (ferric). (b) Ferrous sulfate formed in the Fa_{100} experiments had an Fe/S ratio of 1:1 and a rectangle-shaped boundary but were amorphous inside. (c) Gypsum was identified in the Fa_{71} experiment using SEM. (d) Fe^{II}-Mg-sulfates were identified by TEM with a molar (Fe + Mg)/S ratio of 1:1. (e) Fe^{II}-Mg-sulfates were identified on the surface of the silica beads in the Fa_{50} experiment. (f) The formed Fe^{II}-Mg sulfates showed a clear boundary but were amorphous inside. The sulfate was wrapped by amorphous silica. (g) Fe^{II}-Mg sulfates were identified on the surface of the silica beads in the Fa_{29} experiments. (h) A mixture of Fe^{II}-Mg-sulfates and amorphous silica. Compositional mapping by TEM-EDS of the targets in panel (b, d, f, h) is available in Figure S2 in Supporting Information S1.

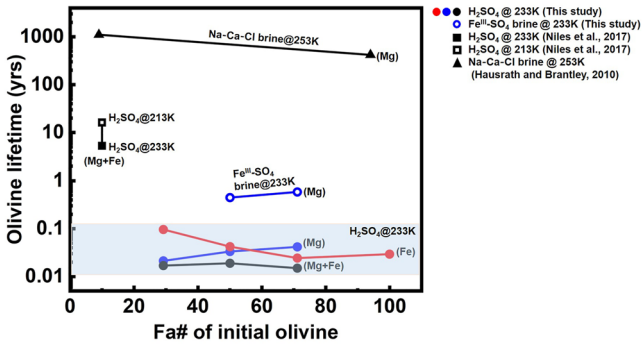

Figure 3. Experimentally estimated particle lifetime of 0.1 mm olivine grains with different Fa# values under cryogenic acidic conditions. The light blue belt highlights the H_2SO_4-233 K conditions in this study, within which the red, blue and black solid dots represent olivine lifetimes estimated using Mg, Fe_T, and the sum of (Mg + Fe_T), respectively. Blue hollow dots represent the $Fe_2(SO_4)_3$-233 K conditions in this study. Black squares represent data from Niles et al. (2017) using San Carlos olivine (Fa_{09}) under H_2SO_4-233 K (solid) and H_2SO_4-213 K (hollow) conditions, comparable to this study. Black triangles represent data from Hausrath and Brantley (2010) using San Carlos olivine (Fa_{09}) and fayalite (Fa_{100}) under acidic Na-Ca-Cl brine-253 K conditions. The pH values were 0.96 (H_2SO_4), 0.41 (Fe^{III}-SO_4 brine), and 0.36 (Na-Ca-Cl brine), measured at 298 K. Note that potentially due to incongruent dissolution of Fe-rich olivine under water-limited conditions, lifetime estimated for Fo-Fa solid solution samples in this study resulted in different trends using different cations. The sum of (Mg + Fe) resulted in a minimum lifetime compared to those calculated using individual Mg or Fe_T. Using the sum of (Mg + Fe), the lifetime of Fe-rich olivine (Fa_{29} to Fa_{71}) is approximately three orders of magnitude faster than that of Mg-rich olivine (San Carlos; Fa_{09}) under comparable conditions. Interacting with acidic Fe^{III}-SO_4 brines, the Fe-rich olivine may survive approximately one order of magnitude longer than those under H_2SO_4 conditions at 233 K. Given that the olivine lifetime can be three orders of magnitude longer in the fields than those estimated in the lab, the lifetime of Fe-rich olivine in the fields is only 10s–100s of years.

0.96 at 298 K), the initial dissolution of olivine in Fe^{III}-SO_4-233 K conditions was hindered, potentially due to high ionic strength and abundant Fe in the initial solution.

Accordingly, the derived lifetime of Fe-rich olivine (i.e., Fa_{29} to Fa_{100}) with a size of 0.1 mm can last only 0.02–0.10 years under H_2SO_4-233 K conditions and 0.45–0.59 years under Fe^{III}-SO_4-233 K conditions (Table 2). The new lifetimes of Fe-rich olivine are about one or two orders of magnitude shorter than previous estimations (Figure 3). Given that the lifetime of natural mineral particles in the fields can last about three orders of magnitude longer than those estimated in the labs (Stopar et al., 2006), Fe-rich olivine can survive in the field for about 20–100 years under cryogenic H_2SO_4 conditions, and about 100s of years under cryogenic acidic Fe^{III}-SO_4 conditions. In general, Fe-rich olivine cannot withstand cryogenic sulfuric weathering and is substantially short-lived from a geological perspective.

4. Implications for Mars

The cryogenic sulfuric weathering scenario differs from freezing fluid alteration due to the extreme acidity and low water-to-rock ratios, which fundamentally influence the dissolution process and secondary phases. At 233 K, the active weathering reagents are concentrated H_2SO_4 in both H_2SO_4 experiments (Beyer et al., 2003) and Fe^{III}-SO_4 experiments (Hennings et al., 2013) and possibly as supercooled ferric sulfate brines in the latter case (Chevrier & Altheide, 2008). Limited amounts but highly concentrated acids can quickly dissolve olivine. The primary weathering products of Fe-rich olivine are Fe^{II}-Mg-sulfates, Fe^{III}-sulfates, gypsum, and amorphous silica. For the Martian surface with bedrock containing olivine, commonly $Fa_{32\text{-}47}$ (Koeppen & Hamilton, 2008), cryogenic sulfuric weathering would efficiently release Fe^{II}, which is temporarily present in the forms of Fe^{II}- and partial Fe^{III}- sulfates, enabling subsequent Fe cycling on the Martian surface. The amorphous silica covering olivine and sulfates is consistent with those widely observed during silicate alteration under cold and acidic conditions, such as hydrated silica on Mars (Tosca & Knoll, 2009), glassy remnant rinds on Martian sediments (Horgan & Bell, 2012), and coatings on terrestrial glaciated volcanic rocks (Rutledge et al., 2018). Gypsum is readily precipitated in a cryogenic sulfuric acid system.

Given the short-lived olivine under both the cryogenic sulfuric weathering scenario and the aqueous acidic sulfate brine scenario (Hausrath & Brantley, 2010; Olsen & Rimstidt, 2007; Stopar et al., 2006), we cannot conclude the primary weathering scenario but provide some inference based on experimental observations. For the Burns Formation at Meridiani (McCollom, 2018), olivine and pyroxene are largely altered and absent in the outcrops (Christensen et al., 2004; Clark et al., 2005). If the cryogenic sulfuric weathering was responsible for the large-scale sulfate deposit at Meridiani and Fa_{40} representing the regional compositions (Christensen et al., 2004), the sulfate products should contain substantial Fe^{II}, which may translocate or oxidize to hematite during subsequent fluid activities (McLennan et al., 2019). Note that the discussion is limited solely to olivine dissolution and does not involve other rock-forming silicates such as pyroxene, which may also contribute cations such as Mg, Ca, Na, and Al to secondary phases, potentially forming other secondary minerals. At Valles Marineris, interior-layered deposits containing interbedded monohydrated and polyhydrated sulfates (Noel et al., 2015; Roach, Mustard, Swayze, et al., 2010), interbedded phyllosilicate-sulfate (Liu et al., 2016), and sulfates and hematite associations (Roach, Mustard, Lane, et al., 2010) are argued to share a similar formation mechanism as Meridiani Terra (Michalski & Niles, 2012; Niles & Michalski, 2009). It is unclear whether olivine and pyroxene are absent within the sulfate-rich layers, but the regional bedrock likely contains olivine and pyroxene, perhaps in the form of basaltic sand coatings (Noel et al., 2015). The cryogenic sulfuric weathering scenario would argue for the precipitation of polyhydrated Fe^{II}-Mg-sulfates. The formed Fe^{II}-Mg sulfates likely inherited the Fe/Mg ratios from the parental olivine (if altering $Fa_{40\text{-}60}$ olivine), so the substantial Fe^{II} would potentially support

the catalyzed dehydration of polyhydrated Mg-sulfate to monohydrate (Steiger et al., 2011; Wang et al., 2009). Further interactions of Fe^{II} with oxidizing agents on the surface under cryogenic conditions would further convert the ferrous sulfate to Fe (oxyhydr)oxides such as goethite, lepidocrocite, schwertmannite, and akaganeite (Mitra et al., 2022). Elevated *T* during burial and diagenesis processes may also facilitate Fe (oxyhydr)oxides formation and result in the separation of Fe from Mg mineral phases. For Fe^{III}, freezing and highly acidic conditions may efficiently suppress Fe^{III} hydrolysis (Marion et al., 2008; Stefansson, 2007). However, the predominant mineral phases for Fe^{III}-SO_4 or Fe^{III}-SO_4-Cl brines under cryogenic conditions are largely unconstrained and require further study. In addition, acidic sulfuric weathering under cryogenic conditions is unlikely to account for the Layered Sulfate unit (LSu) formation in the upper stratified unit at Gale Crater. Diagenetic features, primary Mg- and Ca-sulfates without abundant Fe-sulfates or indication of high acidity, all suggest an evaporative brine environment fluctuating between wet and dry climates (Rapin et al., 2019, 2021), which differs from the scenario discussed in our experiments.

The lifetimes of Fe-rich olivine under cryogenic sulfuric conditions last only 10s to 100s of years for a 0.1 mm grain in the field. If cold and icy conditions persisted in the southern highlands during the late Noachian to the Hesperian and were responsible for forming large-scale sulfate deposits, spatial and temporal restrictions for acid-olivine interactions are essential for preserving Fe-rich olivine throughout cold and icy ancient Mars. One possible way is that the prevailing temperatures are lower than the eutectic points of H_2SO_4 or HCl solutions to prevent acid mobility within the ice body. Another possibility is that the supply of olivine is much greater than the supply of sulfur (e.g., Niles et al., 2017); therefore, the present widespread olivine distribution on Mars may mean that acidic sulfates are not as widespread as previously predicted. Alternatively, sporadic warm events cause melting and efficiently dilute the acidity within the ice body. Impacts and volcanic activities on a generally icy surface would produce sporadic liquid water activities (Bishop et al., 2018; Fastook & Head, 2015; Wordsworth, 2016); however, with elevated temperatures and pressures associated with these events, the olivine alteration scenario would temporally switch from a cold, water-limited regime to a hydrothermal, water-abundant regime, which may lead to different secondary assemblages (e.g., phyllosilicates vs. amorphous silica). For the present Mars, saturated ferric sulfate brine may be present in much of the southern highland at low-mid latitudes (Chevrier & Altheide, 2008). Therefore, cryogenic sulfuric weathering can still affect basaltic materials, but with a limited spatial extent and lower kinetics compared to sulfuric acids on water-abundant or icy ancient Mars.

5. Conclusions

In this study, we experimentally investigate the dissolution of synthetic Fe-rich olivine (Fa_{100}, Fa_{71}, Fa_{50}, and Fa_{29}) for a water-limited cryogenic sulfuric weathering scenario at 233 K. The experimental results are compared with previous studies using forsterite under the same *T*-pH conditions, providing new insights into how the initial Fa# of olivine influences the dissolution rates and how the cryogenic sulfuric weathering scenario affects Fe participation in secondary phases.

1. Forsterite and fayalite in Fo-dominant olivine (Fa# $\leq$ 50) dissolve simultaneously, whereas fayalite dissolution in Fa-dominant olivine (Fa# > 50) is hindered. Some unknown factors at the olivine-solution interfaces may affect fayalite dissolution in Fa-dominant olivine.
2. Fe-rich dissolution under cryogenic sulfuric conditions primarily produces Fe^{II}-Mg-sulfates and amorphous silica with minor ferric sulfates ($Fe_2(SO_4)_3 \cdot nH_2O$) and gypsum. Freezing and acidic conditions significantly suppress Fe^{II} oxidation and Fe^{III} hydrolysis, enhancing Fe mobility and subsequent Fe cycling on the Martian surface. High hydration states are expected for the sulfate evaporites.
3. Fe-rich olivine dissolves two to three orders of magnitude faster than Mg-rich San Carlos olivine, and 0.1 mm Fe-rich olivine grains can survive only 10s to 100s of years under H_2SO_4-233 K conditions. In comparison, Fe-rich olivine can last one order of magnitude longer under acidic Fe^{III}-SO_4-233 K conditions, potentially due to the high ionic strength and abundant Fe of the Fe^{III}-SO_4 solution.
4. If the cryogenic sulfuric weathering scenario was responsible for the large-scale sulfate deposits at Meridiani Planum and Valles Marineris on Mars, the direct sulfate evaporites would be expected to contain substantial Fe^{II} and polyhydrated Fe^{II}-Mg- sulfates. Freezing and acidic conditions significantly suppress Fe^{II} oxidation and Fe^{III} hydrolysis, enhancing Fe mobility and subsequent Fe cycling on the Martian surface.
5. The cryogenic sulfuric weathering scenario greatly challenges the survival of Fe-rich olivine. Thus, spatial and temporal restrictions for acid-olivine interactions are essential for preserving olivine throughout cold and

icy ancient Mars. One possible way is that prevailing temperatures are lower than the eutectic points of H_2SO_4 or HCl solutions to prevent acid mobility within the ice body; another possibility is that insufficient supply of sulfur relative to olivine and the acidic sulfates are not as widespread as previously predicted. Alternatively, sporadic warm events cause melting and efficiently dilute the acidity within the ice body. In addition, ferric sulfate brines may interact with the basaltic materials on present Mars, but within a limited spatial extent and with potentially slower kinetics compared to more icy or water-abundant ancient Mars.

Conflict of Interest

The authors declare no conflicts of interest relevant to this study.

Data Availability Statement

All data generated and analyzed in this study are included in the main article and Supporting Information S1. A complete source data set supporting the paper (i.e., Yu et al., 2022) has also been uploaded to the Science Data Bank.

Acknowledgments

The authors greatly appreciate Paul Niles and the other anonymous reviewer for their constructive suggestions to help us improve this manuscript. This work was supported by the B-type Strategic Priority Program of the Chinese Academy of Sciences (No. XDB41000000) (JZL), Pre-research project on Civil Aerospace Technologies funded by the China National Space Administration (CNSA) (No. D020102) (YYSZ), the Key Research Program of the Chinese Academy of Sciences (ZDBS-SSW-TLC001) (YYSZ), the Program of the Institute of Geology & Geophysics CAS (No. IGGCAS-201905) (SLY), the Science and Technology Planning Project of Guangzhou (No. 202102021184) (YXW), the Innovation Training Program for College Students of Guangdong Province (No. S202111845208) (YXW), The Key Research Program of Frontier Sciences, CAS (No. QYZDY-SSW-DQC028) (JZL), the Beijing Municipal Science and Technology Commission (No. Z181100002918003) (JZL), the Youth Innovation Promotion Association of CAS (Y201867) (XYL), and the National Natural Science Foundation of China (41931077) (XYL).

References

Baccolo, G., Delmonte, B., Niles, P. B., Cibin, G., Di Stefano, E., Hampai, D., et al. (2021). Jarosite formation in deep Antarctic ice provides a window into acidic, water-limited weathering on Mars. *Nature Communications*, *12*(1), 436. https://doi.org/10.1038/s41467-020-20705-z

Beyer, K. D., Hansen, A. R., & Poston, M. (2003). The search for sulfuric acid octahydrate: Experimental evidence. *The Journal of Physical Chemistry A*, *107*(12), 2025–2032. https://doi.org/10.1021/jp026784f

Bishop, J. L., Fairen, A. G., Michalski, J. R., Gago-Duport, L., Baker, L. L., Velbel, M. A., et al. (2018). Surface clay formation during short-term warmer and wetter conditions on a largely cold ancient Mars. *Nature Astronomy*, *2*(3), 206–213. https://doi.org/10.1038/s41550-017-0377-9

Burns, R. G. (1993). Rates and mechanisms of chemical-weathering of ferromagnesian silicate minerals on Mars. *Geochimica et Cosmochimica Acta*, *57*(19), 4555–4574. https://doi.org/10.1016/0016-7037(93)90182-V

Chevrier, V. F., & Altheide, T. S. (2008). Low temperature aqueous ferric sulfate solutions on the surface of Mars. *Geophysical Research Letters*, *35*(22), L22101. https://doi.org/10.1029/2008GL035489

Christensen, P. R., Wyatt, M. B., Glotch, T. D., Rogers, A. D., Anwar, S., Arvidson, R. E., et al. (2004). Mineralogy at Meridiani Planum from the Mini-TES experiment on the Opportunity Rover. *Science*, *306*(5702), 1733–1739. https://doi.org/10.1126/science.1104909

Clark, B. C., Morris, R. V., McLennan, S. M., Gellert, R., Jolliff, B., Knoll, A. H., et al. (2005). Chemistry and mineralogy of outcrops at Meridiani Planum. *Earth and Planetary Science Letters*, *240*(1), 73–94. https://doi.org/10.1016/j.epsl.2005.09.040

Dehouck, E., Gaudin, A., Mangold, N., Lajaunie, L., Dauzeres, A., Grauby, O., & Le Menn, E. (2014). Weathering of olivine under CO_2 atmosphere: A Martian perspective. *Geochimica et Cosmochimica Acta*, *135*, 170–189. https://doi.org/10.1016/j.gca.2014.03.032

Fastook, J. L., & Head, J. W. (2015). Glaciation in the Late Noachian Icy Highlands: Ice accumulation, distribution, flow rates, basal melting, and top-down melting rates and patterns. *Planetary and Space Science*, *106*, 82–98. https://doi.org/10.1016/j.pss.2014.11.028

Gaudin, A., Dehouck, E., Grauby, O., & Mangold, N. (2018). Formation of clay minerals on Mars: Insights from long-term experimental weathering of olivine. *Icarus*, *311*, 210–223. https://doi.org/10.1016/j.icarus.2018.01.029

Hausrath, E. M., & Brantley, S. L. (2010). Basalt and olivine dissolution under cold, salty, and acidic conditions: What can we learn about recent aqueous weathering on Mars? *Journal of Geophysical Research*, *115*(E12), E12001. https://doi.org/10.1029/2010JE003610

Hennings, E., Zürner, P., Schmidt, H., & Voigt, W. (2013). Freezing temperatures of aqueous iron(III) sulfate solutions and crystallization of a new acidic water-rich sulfate. *Icarus*, *226*(1), 268–271. https://doi.org/10.1016/j.icarus.2013.05.023

Hoefen, T. M., Clark, R. N., Bandfield, J. L., Smith, M. D., Pearl, J. C., & Christensen, P. R. (2003). Discovery of olivine in the Nili Fossae region of Mars. *Science*, *302*(5645), 627–630. https://doi.org/10.1126/science.1089647

Horgan, B., & Bell, J. F., III. (2012). Widespread weathered glass on the surface of Mars. *Geology*, *40*(5), 391–394. https://doi.org/10.1130/g32755.1

Hurowitz, J. A., McLennan, S. M., Tosca, N. J., Arvidson, R. E., Michalski, J. R., Ming, D. W., et al. (2006). In situ and experimental evidence for acidic weathering of rocks and soils on Mars. *Journal of Geophysical Research*, *111*(E2), E02S19. https://doi.org/10.1029/2005JE002515

Koeppen, W. C., & Hamilton, V. E. (2008). Global distribution, composition, and abundance of olivine on the surface of Mars from thermal infrared data. *Journal of Geophysical Research*, *113*(E5), E05001. https://doi.org/10.1029/2007JE002984

Lasaga, A. C. (1998). *Kinetic theory in the Earth Sciences*. Princeton University Press. https://doi.org/10.1017/S0016756800234614

Liu, Y., Glotch, T. D., Scudder, N. A., Kraner, M. L., Condus, T., Arvidson, R. E., et al. (2016). End-member identification and spectral mixture analysis of CRISM hyperspectral data: A case study on southwest Melas Chasma, Mars. *Journal of Geophysical Research: Planets*, *121*(10), 2004–2036. https://doi.org/10.1002/2016JE005028

Marion, G. M., Kargel, J. S., & Catling, D. C. (2008). Modeling ferrous-ferric iron chemistry with application to Martian surface geochemistry. *Geochimica et Cosmochimica Acta*, *72*(1), 242–266. https://doi.org/10.1016/j.gca.2007.10.012

McCollom, T. M. (2018). Geochemical trends in the Burns formation layered sulfate deposits at Meridiani Planum, Mars, and implications for their origin. *Journal of Geophysical Research: Planets*, *123*(9), 2393–2429. https://doi.org/10.1029/2018JE005718

McLennan, S. M., Grotzinger, J. P., Hurowitz, J. A., & Tosca, N. J. (2019). The sedimentary cycle on early Mars. *Annual Review of Earth and Planetary Sciences*, *47*(1), 91–118. https://doi.org/10.1146/annurev-earth-053018-060332

McSween, H. Y., Jr. (2015). Petrology on Mars. *American Mineralogist*, *100*(11–12), 2380–2395. https://doi.org/10.2138/am-2015-5257

McSween, H. Y., Ruff, S. W., Morris, R. V., Gellert, R., Klingelhöfer, G., Christensen, P. R., et al. (2008). Mineralogy of volcanic rocks in Gusev crater, Mars: Reconciling Mössbauer, Alpha particle X-ray spectrometer, and Miniature thermal emission spectrometer spectra. *Journal of Geophysical Research*, *113*(E6), 2169–9097. https://doi.org/10.1029/2007JE002970

Michalski, J., & Niles, P. B. (2012). Atmospheric origin of Martian interior layered deposits: Links to climate change and the global sulfur cycle. *Geology*, *40*(5), 419–422. https://doi.org/10.1130/g32971.1

Mitra, K., Moreland, E. L., Knight, A. L., & Catalano, J. G. (2022). Rates and products of iron oxidation by Chlorate at low temperatures (0 to 25°C) and implications for Mars geochemistry. *ACS Earth and Space Chemistry*, *6*(2), 250–260. https://doi.org/10.1021/acsearthspacechem.1c00379

Niles, P. B., & Michalski, J. (2009). Meridiani Planum sediments on Mars formed through weathering in massive ice deposits. *Nature Geoscience*, *2*(3), 215–220. https://doi.org/10.1038/ngeo438

Niles, P. B., Michalski, J., Ming, D. W., & Golden, D. C. (2017). Elevated olivine weathering rates and sulfate formation at cryogenic temperatures on Mars. *Nature Communications*, *8*(1), 998. https://doi.org/10.1038/s41467-017-01227-7

Noel, A., Bishop, J. L., Al-Samir, M., Gross, C., Flahaut, J., McGuire, P. C., et al. (2015). Mineralogy, morphology and stratigraphy of the light-toned interior layered deposits at Juventae Chasma. *Icarus*, *251*, 315–331. https://doi.org/10.1016/j.icarus.2014.09.033

Olsen, A. A., & Rimstidt, J. D. (2007). Using a mineral lifetime diagram to evaluate the persistence of olivine on Mars. *American Mineralogist*, *92*(4), 598–602. https://doi.org/10.2138/am.2007.2462

Qi, C., Zhao, Y. H., Zimmerman, M. E., Kim, D., & Kohlstedt, D. L. (2021). Evolution of microstructural properties in sheared iron-rich olivine. *Journal of Geophysical Research: Solid Earth*, *126*(3), e2020JB019629. https://doi.org/10.1029/2020jb019629

Rapin, W., Dromart, G., Rubin, D., Deit, L. L., Mangold, N., Edgar, L. A., et al. (2021). Alternating wet and dry depositional environments recorded in the stratigraphy of Mount Sharp at Gale crater, Mars. *Geology*, *49*(7), 842–846. https://doi.org/10.1130/g48519.1

Rapin, W., Ehlmann, B. L., Dromart, G., Schieber, J., Thomas, N. H., Fischer, W. W., et al. (2019). An interval of high salinity in ancient Gale crater lake on Mars. *Nature Geoscience*, *12*(11), 889–895. https://doi.org/10.1038/s41561-019-0458-8

Rimstidt, J. D., & Newcomb, W. D. (1993). Measurement and analysis of rate data-the rate of reaction of ferric iron with pyrite. *Geochimica et Cosmochimica Acta*, *57*(9), 1919–1934. https://doi.org/10.1016/0016-7037(93)90084-a

Roach, L. H., Mustard, J. F., Lane, M. D., Bishop, J. L., & Murchie, S. L. (2010). Diagenetic haematite and sulfate assemblages in Valles Marineris. *Icarus*, *207*(2), 659–674. https://doi.org/10.1016/j.icarus.2009.11.029

Roach, L. H., Mustard, J. F., Swayze, G., Milliken, R. E., Bishop, J. L., Murchie, S. L., & Lichtenberg, K. (2010). Hydrated mineral stratigraphy of Ius Chasma, Valles Marineris. *Icarus*, *206*(1), 253–268. https://doi.org/10.1016/j.icarus.2009.09.003

Rutledge, A. M., Horgan, B. H. N., Havig, J. R., Rampe, E. B., Scudder, N. A., & Hamilton, T. L. (2018). Silica dissolution and precipitation in glaciated volcanic environments and implications for Mars. *Geophysical Research Letters*, *45*(15), 7371–7381. https://doi.org/10.1029/2018gl078105

Stefansson, A. (2007). Iron(III) hydrolysis and solubility at 25°C. *Environmental Science & Technology*, *41*(17), 6117–6123. https://doi.org/10.1021/es070174h

Steiger, M., Linnow, K., Ehrhardt, D., & Rohde, M. (2011). Decomposition reactions of magnesium sulfate hydrates and phase equilibria in the $MgSO_4$–H_2O and Na^+–Mg^{2+}–Cl^-–SO_4^{2-}–H_2O systems with implications for Mars. *Geochimica et Cosmochimica Acta*, *75*(12), 3600–3626. https://doi.org/10.1016/j.gca.2011.03.038

Stopar, J. D., Jeffrey Taylor, G., Hamilton, V. E., & Browning, L. (2006). Kinetic model of olivine dissolution and extent of aqueous alteration on Mars. *Geochimica et Cosmochimica Acta*, *70*(24), 6136–6152. https://doi.org/10.1016/j.gca.2006.07.039

Tosca, N. J., & Knoll, A. H. (2009). Juvenile chemical sediments and the long term persistence of water at the surface of Mars. *Earth and Planetary Science Letters*, *286*(3–4), 379–386. https://doi.org/10.1016/j.epsl.2009.07.004

Wang, A., Freeman, J. J., & Jolliff, B. L. (2009). Phase transition pathways of the hydrates of magnesium sulfate in the temperature range 50°C to 5°C: Implication for sulfates on Mars. *Journal of Geophysical Research*, *114*(E4), E04010. https://doi.org/10.1029/2008je003266

Wordsworth, R. D. (2016). The climate of early Mars. *Annual Review of Earth and Planetary Sciences*, *44*(1), 381–408. https://doi.org/10.1146/annurev-earth-060115-012355

Yu, X. W., Zhao, Y. Y. S., Wu, Y. X., Qi, C., Li, D. D., Lin, H. L., et al. (2022). Dataset for cryogenic sulfuric weathering and challenges for preserving iron-rich olivine on cold and icy Mars [Dataset]. Science Data Bank. https://doi.org/10.57760/sciencedb.06446

Zhao, Y.-H., Zimmerman, M. E., & Kohlstedt, D. L. (2009). Effect of iron content on the creep behavior of olivine: 1. Anhydrous conditions. *Earth and Planetary Science Letters*, *287*(1–2), 229–240. https://doi.org/10.1016/j.epsl.2009.08.006